

Exploiting potential energy storage for cyclic manipulation: An analysis for elastic dribbling with an anthropomorphic robot

Sami Haddadin, Kai Krieger, Mirko Kunze, and Alin Albu-Schäffer

Abstract—For achieving dynamic manipulation capabilities that are comparable to human performance in terms of speed, energetic properties, and robustness, intrinsic elasticity is widely proposed as a necessary robot design element. In this paper we show how passive compliance can be exploited for a 6-degree-of-freedom (DoF) cyclic ball dribbling task with a 7-DoF articulated Cartesian impedance controlled DLR Lightweight Robot III [1]. For this, the robot is equipped with an elastic hand, which extends the contact time and therefore, also enlarges both, observability and controllability of the ball. We show via simulation and experiment that it is possible to achieve a stable dynamic cycle based on a solid 1 DoF analysis from [2] for the main axis together with control strategies for the secondary translations and rotations of the task. The scheme allows also the continuous tracking of a desired dribbling height and horizontal position. As a human is able to dribble blindly, we decided to solve the task by force sensing only, i.e. no vision is used for our approach, however, could be easily incorporated.

I. INTRODUCTION

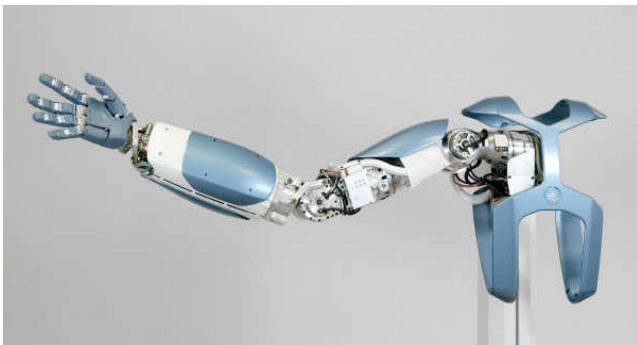


Fig. 1. The DLR hand arm system.

Hybrid object manipulation¹ has been investigated for many years. Robot dribbling is such a task and was first introduced in [3]. The authors used a half-cylindrical tube for mapping the system to a 2-D system. The control is reactive and pushes the ball only downwards if a contact is detected while, depending on the contact position, a spin type effect is also applied². [4] utilizes a high-speed multi-fingered hand for dribbling a ping-pong ball with high-speed vision. [5] introduced a basketball playing industrial robot,

The first two authors contributed equally to the work. S. Haddadin, K. Krieger, Mirko Kunze and A. Albu-Schäffer are with the Institute of Robotics and Mechatronics, DLR - German Aerospace Center, Wessling, Germany, contact: sami.haddadin@dlr.de

¹We refer to discrete switching between contact and non-contact situations, where hybrid systems theory can be applied.

²As the referenced publication is only a video, it is not exactly clear which degrees of freedom (DoF) are purposely controlled.

utilizing a solid plate as hand. The control relies mainly on the ball tracking vision system for stabilizing reactions. In [6] some theoretical analysis was given for using an elastic contact element based on an optimal control trajectory.

A dribbling related task is the classical juggling problem, which was first treated in [7]. In [8] the first blindly juggling robot was described. [9] used only a linear motor for juggling without the need of active ball tracking, as the lateral motion is stabilized by the shape of a juggling paddle. In [9] the authors compared an \mathcal{H}_2 optimal controller with their previous open-loop control, which turned out to have similar performance characteristics.

In this paper we provide insights into the problem of *elastic* dribbling. Generally, it is very suitable to further understand how intrinsic elasticity enable high-performance and energy efficiency during highly dynamic and repetitive tasks (e.g. in throwing [10], walking [11], and batting [12]). These applications pose high demands on the robot in terms of speed, dexterity, and robustness.

In this paper we present the design of a full 6-DoF elastic dribbling controller and perform simulations and experiments for its validation. We consider the problem of a rather stiff Cartesian impedance controlled lightweight arm that is equipped with an intrinsically compliant hand. This intrinsically elastic part of the robot dynamically stores and releases elastic energy that is transferred between ball and robot. The work presented in this paper intends to lay ground on our future work for full Variable Impedance Actuation (VIA) arms. Recently, we have built a full 7-DoF VIA arm at DLR [13] (see Fig. 1) for which the extension of the methods developed in the present paper is certainly the next step to take. The ground work for our presented analysis is given in [2], where we analyze the stability, power characteristics, and robustness of a 1-DoF elastic dribbling system³. There, we also design a stable observation method for tracking the ball based on contact force measurement only. The extension to the full dimensional problem enables also the stable tracking of dribbling at a desired position and height⁴.

The paper is organized as follows. The extension of the 1-DoF system from [2] to full 6-DoF is done in Sec. II. Section III extends the observer from [2] to all three translations and adds a control scheme for the lateral ball motion. Human dribbling experiments, simulations, and dribbling experiments with a 7-DoF DLR Lightweight Robot III (LWR-III) [1] are presented in Sec. IV. The paper concludes with

³Please note that you may download the preprint of the paper from www.safe-robots.com/dribbling.html.

⁴Actually, our scheme allows also to adjust the dribbling frequency and amplitude. However, this is omitted for brevity

Sec. V.

Videos of the robot dribbling, showing the performance of our controller, can be viewed at www.safe-robots.com/dribbling.html or in the video attachment.

II. MODELING

In this section we outline the ball and hand model suitable for 6-DoF dribbling task. A schematic view of the model is depicted in Fig. 2. In reality we use three fingers that are mounted along one common plane, cf. Fig. 3. The fingers are made of spring steel, while for impact damping issues foam is glued to them.

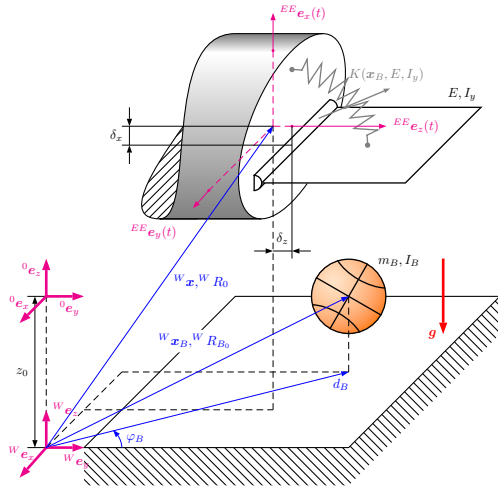


Fig. 2. Definitions and conventions for the overall hand-ball model.



Fig. 3. Elastic dribbling hand used for the experiments with the DLR Lightweight-Robot III.

In the modeling part, we assume them to be massless and use only their respective spring characteristics, cf. Fig. 2. Both bodies are described by their respective position and orientation. The relevant frames are the end-effector frame $\{EE\}$, the world frame $\{W\}$ (located on the floor), and the base frame $\{0\}$ (above the world frame). The spring mounting is translated into the $\{EE\}$ frame by the offsets δ_z and δ_x .

In the following, we derive a suitable ball model and then show how to obtain the relevant forces acting on the ball. All

vectors will be expressed in $\{W\}$ unless specified otherwise. Hence, we drop the index for this frame.

A. Ball model

The ball is modeled as a free body with the gravity vector \mathbf{g} and the contact force \mathbf{F}_B acting on its perimeter. It is described by three translational coordinates $\mathbf{x}_B = [x_B \ y_B \ z_B]^T$, the respective velocity $\dot{\mathbf{x}}_B$, the quaternion $\boldsymbol{\xi}_B = [q_0 \ q_1 \ q_2 \ q_3]^T$, and three rotational velocities $\boldsymbol{\omega}_B = [\alpha_B \ \beta_B \ \gamma_B]^T$ about the axes of $\{W\}$. Its equation of motion is

$$\begin{bmatrix} \ddot{\mathbf{x}}_B \\ \dot{\boldsymbol{\xi}}_B \\ \dot{\boldsymbol{\omega}}_B \end{bmatrix} = \begin{bmatrix} \frac{1}{m_B} \mathbf{F}_B + \mathbf{g} \\ \frac{1}{2} \mathbf{Q}(\boldsymbol{\xi}) \boldsymbol{\omega}_B \\ \mathbf{I}_B^{-1} (\mathbf{r}_B \times \mathbf{F}_B) \end{bmatrix}, \quad (1)$$

with \mathbf{r}_B being the vector from the ball center to the force application point, m_B the ball mass, and \mathbf{I}_B the ball inertia tensor, which is diagonal due to the ball's rotational symmetry. $\mathbf{Q}(\boldsymbol{\xi})$ is a matrix that maps Cartesian velocities $\boldsymbol{\omega}_B$ to quaternion velocities [14]. The calculation of the force \mathbf{F}_B for the different phases is shown in the following paragraphs.

For the control presented later it is useful to have the translational coordinates also in cylindrical coordinates $\mathbf{x}_{BC} = [\varphi_B \ d_B \ z_B]^T$, see Fig. 2. These are obtained via

$$\mathbf{x}_{BC} = \begin{bmatrix} \varphi_B \\ d_B \\ z_B \end{bmatrix} = \begin{bmatrix} \arctan_2(-x_B, y_B) \\ \sqrt{x_B^2 + y_B^2} \\ z_B \end{bmatrix}. \quad (2)$$

B. Floor contact

The ball is in floor contact if

$$z_B \leq r_B, \quad (3)$$

with r_B being the ball radius. The contact force consists of two components. \mathbf{F}_{FC_n} is the normal force and \mathbf{F}_{FC_t} the force tangential to the floor plane.

1) *Normal force*: The normal force is calculated by a Hunt-Crossley Model [15] that is chosen to be

$$\mathbf{F}_{FC_n} = [-K_F(z_B - r_B) - D_F(z_B - r_B)\dot{z}_B] \mathbf{e}_z, \quad (4)$$

with K_F being the stiffness constant and D_F the damping constant.

2) *Tangential force*: The physical effect caused by the tangential force is that the relative velocity between ball and floor fades away over the contact. This is taken into account by a lumped LuGre model [16], which is given as

$$\dot{s} = |\mathbf{v}_{FC_r}| - \frac{\sigma_0 |\mathbf{v}_{FC_r}|}{g(\mathbf{v}_{FC_r})} s \quad (5)$$

$$\mathbf{F}_t = (\sigma_0 s + \sigma_1 \dot{s} + \sigma_2 |\mathbf{v}_{FC_r}|) |\mathbf{F}_{FC_n}|, \quad (6)$$

with

$$g(\mathbf{v}_{FC_r}) = \mu_c + (\mu_s - \mu_c) e^{-|\mathbf{v}_{FC_r}|/v_s} \quad (7)$$

s is the slip between ball and floor, σ_0 the rubber longitudinal lumped stiffness, σ_1 the rubber longitudinal lumped damping, σ_2 the viscous relative damping, μ_c the normalized Coulomb friction, μ_s the normalized static friction, v_s the

Stribeck relative velocity, F_n the normal force, v_{FC_r} the relative velocity. The steady-state friction/slip characteristic is captured by α . In our simulations we use following numerical values

$$\begin{aligned} & [\sigma_0 \ \sigma_1 \ \sigma_2 \ \mu_c \ \mu_s \ v_s \ \alpha] \\ & = [1000 \text{ N/m} \ 100 \text{ Ns/m} \ 0.1 \text{ Ns/m} \ 0.8 \ 0.9 \ 20 \text{ m/s} \ 1]. \end{aligned} \quad (8)$$

The parameters are chosen such that the friction reaches its steady state in the short floor contact time. The Coulomb friction parameters are given in [17]. The relative velocity sought after is calculated by

$$v_{FC_r} = [0 \ e_y \ e_z]^T \dot{x}_B + [0 \ 0 \ -r_B]^T \times \omega_B. \quad (9)$$

Furthermore, (9) provides also the direction of the tangential force, as it acts in opposite direction to the relative velocity.

C. Hand model

The robot end-effector will later be commanded via a desired frame fed to a Cartesian impedance controller (see Sec. IV). The rotation matrix is described by a well chosen set of Euler angles in the sense of the task, whose rotation order is depicted in Fig. 4.

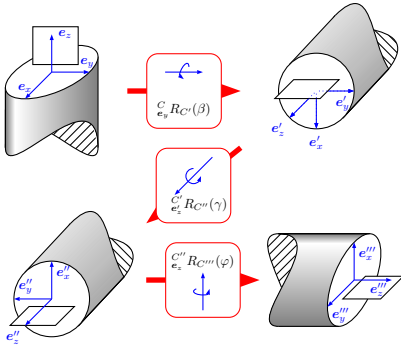


Fig. 4. Rotation order for commanding the orientation of the of the robot hand, which is sketched as a plate.

The first coordinate system $\{C\}$ is collinear to the base frame. The first rotation acts around the y -axis and is later used for controlling the ball along the d_B coordinate. Thereafter, the coordinate system is rotated around the new z -axis, which will be used for controlling the ball along the φ_B coordinate. The last rotation is around the z -axis of the base frame and is used for tracking the ball position.

D. Hand contact

The hand contact is calculated similarly to the floor contact. Therefore, it is advantageous to use the position vector of the ball expressed in $\{EE\}$. The condition for hand contact is

$${}^{EE}x_B \geq \delta_x + r_B. \quad (10)$$

We assume the absence of damping in the hand as the fingers are made of spring steel. Hence, we get

$${}^{EE}\mathbf{F}_{HC_n} = K(\mathbf{x}_B, E, I_y)(-{}^{EE}x_B + \delta_x + r_B){}^{EE}e_x \quad (11)$$

for the normal direction of the contact. The stiffness $K(\mathbf{x}_B, E, I)$ is calculated from the linear theory on Bernoulli beams, see Fig. 5. The force F denotes the force that is applied by the ball. This causes two reactions M_R and N , as well as the bending line $w(z)$, which is calculated by [18]

$$EI_y \frac{d^2 w(z)}{dz^2} = -M_y(z). \quad (12)$$

E is the modulus of elasticity, I_y is the geometrical moment of inertia around the y -axis, and M_y is the bending moment around y , which is obtained by

$$M_y(z) = \underbrace{F z_F}_{=M_R} - \underbrace{F}_{=N} z + \begin{cases} 0 & \text{for } z \leq z_F \\ F(z - z_F) & \text{for } z > z_F \end{cases}. \quad (13)$$

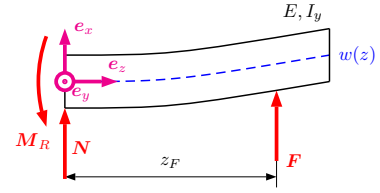


Fig. 5. Calculation of spring stiffness K seen at the contact point.

Evaluating (12) at z_F results in a relation between the force and the bending at z_F as

$$F = \underbrace{\frac{EI_y}{3z_F^3}}_K w(z_F). \quad (14)$$

Therewith, the stiffness K seen at the contact point is known. The tangential direction of the force is calculated analogue to Sect. II-B by utilizing a LuGre model. The full contact force wrench is denoted by $\mathcal{F}_{ext} = [{}^{EE}\mathbf{F}_{ext}^T \ {}^{EE}\mathbf{M}_{ext}^T]^T$.

E. Elastic joint robot model

In this paper, we show simulations, which consider the robot to be a position/velocity source but also simulations and experiments that take the full dynamic model and control of a Cartesian impedance controlled robot into consideration. Therefore, we introduce the underlying set of equations describing the robot dynamics next. The controller is outlined in Sec. III-C.

Due to the lightweight design of the LWR-III it is not sufficient to model the robot by a second-order rigid body model. The non negligible joint elasticity between motor and link inertia caused by the Harmonic Drive gears and the joint torque sensor has to be taken into account into the model equation. For such a robot the following flexible joint model can be assumed [19]:

$$M(\mathbf{q})\ddot{\mathbf{q}} + C(\mathbf{q}, \dot{\mathbf{q}})\dot{\mathbf{q}} + \mathbf{g}(\mathbf{q}) = \boldsymbol{\tau}_J + \boldsymbol{\tau}_{ext} \quad (15)$$

$$B\ddot{\boldsymbol{\theta}} + \boldsymbol{\tau}_J = \boldsymbol{\tau}_m \quad (16)$$

$$\boldsymbol{\tau}_J = K_J(\boldsymbol{\theta} - \mathbf{q}), \quad (17)$$

with \mathbf{q} being the link side position, $\boldsymbol{\theta}$ the motor position, $\boldsymbol{\tau}_J$ the elastic joint torque, $M(\mathbf{q})$ the mass matrix, $C(\mathbf{q}, \dot{\mathbf{q}})$ the centripetal and Coriolis vector, $\mathbf{g}(\mathbf{q})$ the gravity vector, $K_J = \text{diag}\{K_{J,i}\}$ the diagonal positive definite joint stiffness matrix, and $B = \text{diag}\{B_i\}$ the diagonal positive definite motor inertia matrix⁵. The external joint torque is generated by the ball contact wrench measured in the wrist sensor via $\boldsymbol{\tau}_{ext} = J^{T EE} \mathcal{F}_{ext}$, with J being the $\{EE\}$ Jacobian of the manipulator.

In the next section we give an overview on the extension of the ball observer from [2]. Furthermore, we outline how to control the ball for achieving a robust dribbling cycle.

III. CONTROL

Our aim is to dribble blindly with force feedback only. In order to cope with process uncertainties, we need to reliably observe the ball position. Based on the ball observation it is possible to design a control law that is able to stabilize the dribbling cycle.

A. Ball observer

In this paper we observe the ball with the method described in [2]. Based on the measurement of contact forces⁶, a sliding mode observer can be set up for the estimation of the vertical ball motion. The other translations x_B and y_B can be observed by a similar scheme. It consists of a sliding mode observer [20] during hand contact and a model based prediction in the remaining non-contact phase⁷. The observer input is the ball position obtained from measured wrenches in the wrist frame (end-effector frame). Since we assume negligible contact moments, we can use the principle of solidification for calculating the ball position, i.e. there has to be a straight line on which no moments are acting [21]. This straight line ${}^{EE}\mathbf{r}_S(\lambda)$ can be found by solving

$${}^{EE}\mathbf{M}_{ext} = {}^{EE}\mathbf{r}_S(\lambda) \times {}^{EE}\mathbf{F}_{ext} \quad (18)$$

for ${}^{EE}\mathbf{r}_S(\lambda)$, with λ being the curve parameter of the straight line. Therewith, the contact point ${}^{EE}\mathbf{r}_c$ is obtained from the intersection of ${}^{EE}\mathbf{r}_S(\lambda)$ with the finger plane ${}^{EE}x = -\delta_x$. ${}^{EE}\mathbf{M}_{ext}$ is the measured contact moment and ${}^{EE}\mathbf{F}_{ext}$ the measured force vector. With ${}^{EE}\mathbf{r}_c$ and (14) we obtain the stiffness at the point of contact. Hence, with the direction of the straight line, which is given by ${}^{EE}\mathbf{F}_{ext}$ we get the ball position as

$${}^{EE}\mathbf{r}_B = {}^{EE}\mathbf{r}_c + \frac{{}^{EE}\mathbf{F}_{ext}}{|{}^{EE}\mathbf{F}_{ext}|} \left(-r_B + \frac{|{}^{EE}\mathbf{F}_{ext}|}{K({}^{EE}\mathbf{r}_c, \mathbf{E}, I_y)} \right). \quad (19)$$

This quantity takes the ball radius r_B and the spring bending into account. As the sliding mode observer tends to scattering, we filter the observed ball position with a PT3 element prior to using it in the feedback loop (see Sec. III-B). Therewith, we get a reference that is three times continuously differentiable, i.e. only jerk scatters.

⁵Please note that for sake of clarity we omit the joint damping and motor side friction (they are, however, taken into consideration for the simulations).

⁶In this paper we utilize a JR3 6 DoF force/torque sensor mounted in the robot wrist.

⁷For the details on the observer design please refer to [2].

The measured force signal contains not only contact forces, but also high frequency noise, disturbances due to the oscillations of the intrinsically compliant fingers, and inertial effects of the load seen by the sensor while performing the dribbling motion. Therefore, we need to compensate the most significant effects for reliably estimating the contact position of the ball. In order to eliminate the high-frequency noise, we simply filter the raw signal with a PT2 element. As the finger oscillations have only a small amplitude and the associated frequency is very close to the frequency spectrum of the contact force, we neglect this effect. Because the desired dribbling motion demands very high acceleration, inertial forces due to the load mass are the most significant disturbance. Since acceleration cannot be obtained from currently available position sensors via twice numerical differentiation, we need an appropriate method to observe the Operational space acceleration of the robot flange.

In order to get a reliable acceleration estimate, we use a nonlinear disturbance observer according to [22]. It is defined as

$$\hat{\ddot{\mathbf{q}}} = M^{-1}(\boldsymbol{\tau} - \mathbf{n}(\mathbf{q}, \dot{\mathbf{q}}) - K_O(\hat{\mathbf{q}} - \dot{\mathbf{q}})), \quad (20)$$

where $\hat{\mathbf{q}}$ denotes the observed joint position, $\mathbf{n}(\mathbf{q}, \dot{\mathbf{q}}) = C(\mathbf{q}, \dot{\mathbf{q}})\dot{\mathbf{q}} + \mathbf{g}(\mathbf{q})$, and K_O is the observer gain matrix. With this we get an observation of $\ddot{\mathbf{q}}$ that relies on the measurement of the joint position and velocity only. Figure 6 depicts the according signal flow diagram.

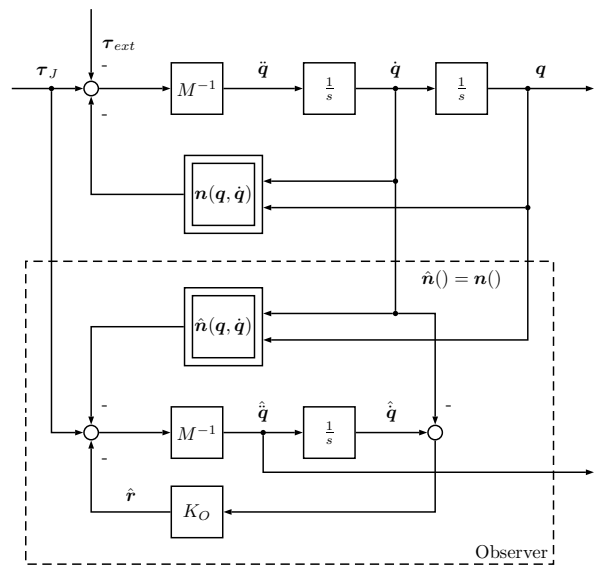


Fig. 6. Velocity disturbance observer.

With the observed joint accelerations we can easily obtain the Cartesian accelerations and consequently also the forces due to load accelerations via

$$\hat{\mathbf{x}} = \hat{J}\hat{\ddot{\mathbf{q}}} + \dot{\hat{J}}\hat{\dot{\mathbf{q}}}. \quad (21)$$

B. Control

In general, we intend to stabilize the ball at a steady point $\mathbf{x}_{BC,des}$ (in fact at a projection on the horizontal plane). For the vertical motion we refer to the methods developed in [2],

where we give a stability proof and a robustness analysis for the 1 DoF system that is excited by the vertical trajectory

$$z(t) = \begin{cases} A \sin\left(\frac{5\pi}{4T}t\right) + z_0 & \text{for } t \in \left[0; \frac{4}{5}T\right] \\ -\frac{1}{4}A \sin\left(\frac{5\pi}{T}t\right) + z_0 & \text{for } t \in \left[\frac{4}{5}T; T\right]. \end{cases} \quad (22)$$

In this paper we incorporate also the vertical ball motion⁸. For stabilizing the lateral motion the hand needs to follow the observed ball position from Sec. III-A. Since we want to control the ball in cylindrical coordinates (see Fig. 2), the desired position is

$$\begin{bmatrix} x_{des} \\ y_{des} \\ \varphi_{des} \end{bmatrix} = \begin{bmatrix} -(d_B - \Delta_H) - \sin(\varphi_B) \\ (d_B - \Delta_H) \cos(\varphi_B) \\ \varphi_B \end{bmatrix}, \quad (23)$$

with Δ_H being an offset from the $\{EE\}$ coordinate system to the middle of the finger. For attracting the ball to $x_{B_{C_{des}}}$ we use a simple PID control for the two remaining hand rotations:

$$\begin{aligned} \beta_{des} &= K_{P\beta}(d_{B_{des}} - d_B) \\ &+ K_{I\beta} \int_0^t (d_{B_{des}} - d_B) d d_B \\ &+ K_{D\beta}(\dot{d}_{B_{des}} - \dot{d}_B), \end{aligned} \quad (24)$$

$$\begin{aligned} \gamma_{des} &= K_{P\gamma}(\varphi_{B_{des}} - \varphi_B) \\ &+ K_{I\gamma} \int_0^t (\varphi_{B_{des}} - \varphi_B) d \varphi_B \\ &+ K_{D\gamma}(\dot{\varphi}_{B_{des}} - \dot{\varphi}_B), \end{aligned} \quad (25)$$

with K_{xx} being the respective gains for the PID control.

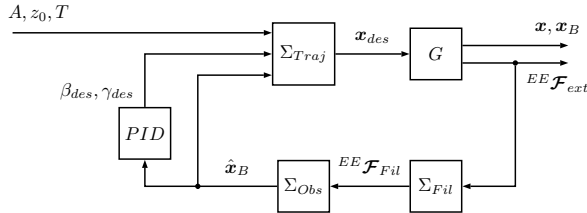


Fig. 7. The overall dribbling controller consists of the trajectory generator, the ball observer, and the wrench filter. The trajectory generator takes into account the ball estimation coming from the ball observer, which is purely generated from interaction force measurement.

The overall structure of the closed loop system is shown in Fig. 7. A, z_0 and T are specified by the user for the given parameters of the z -axis trajectory (stable ranges according to [2]). G denotes the robot ball model. Its measured outputs are the contact force wrench ${}^{EE}\mathcal{F}_{ext}$ and the robot position x . ${}^{EE}\mathcal{F}_{ext}$ is filtered in Σ_{Fil} . This filtered signal ${}^{EE}\mathcal{F}_{Fil}$ is fed to the observer Σ_{Obs} in order to construct the position estimate \hat{x}_B . This is then used in the control laws given by (24) and (25).

In order to prepare future experiments with the DLR hand-arm system, we decided to interface the LWR-III from the

⁸For this, we still have to develop a stability analysis in future work.

trajectory generation side via Cartesian impedance control. This can be considered as the closest approximation of a full passively compliant system that can be realized with the LWR-III. Therefore, we shortly summarize the main characteristics of the used scheme.

C. Cartesian impedance controller

Based on the elastic joint model described in Sec. II-E following controller structure⁹ is used for controlling the full robot dynamics simulation and the real-robot. It enables high performance Cartesian impedance control at a rate of 1 kHz with velocity feed forward. The closed form solution of the overall scheme can be written as

$$u = -J(\bar{q})^T (K_x \tilde{x}(\bar{q}) + D_x \dot{\tilde{x}}(\bar{q})) + \bar{g}(\theta), \quad (26)$$

where u is a new control input (instead of motor torque) for a lower level full state feedback controller (incorporation of motor position, joint torque, and their respective derivatives) [23]. The impedance control is designed with following quantities. $K_x, D_x \in \mathbb{R}^{m \times m}$ are the diagonal positive definite desired stiffness and damping matrix. $x_d \in \mathbb{R}^m$ is the desired tip position in Cartesian coordinates, which is commanded via the control law described in the previous subsection, and $\tilde{x}(\bar{q}) = x(\bar{q}) - x_d$. $x(\bar{q}) = T(\bar{q})$ is the forward kinematics map. $\bar{q} = h^{-1}(\theta)$ is the static equivalent of q . The gravity compensation term $\bar{g}(\theta)$ is a function of the motor position and is designed in such way, that it provides exact gravity compensation in static case. In the simulation and experiments presented later we selected K_x to be $K_x = \text{diag}\{1500 \ 1500 \ 1500 \ 200 \ 200 \ 200\}$ (translational stiffness in N/m and rotational stiffness in Nm/rad).

In the following section we first present human dribbling measurement data obtained via passive marker tracking. Furthermore, we show some simulation results based on the model from Sec. II and Sec. III. Finally, the experimental confirmation of the elastic dribbling controller is given.

IV. SIMULATIONS AND EXPERIMENTS

A. Human dribbling measurement

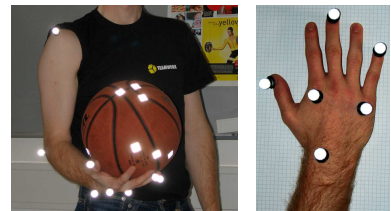


Fig. 8. Setup and marker positions for the human dribbling experiments.

In order to understand the speed requirements needed for human dribbling, we carried out some experiments in which a human arm and the ball were tracked with a Vicon tracking system. The sampling rate is 180 Hz and eight cameras were used to have good scene coverage. Figure 8 depicts the locations of the tracked markers that were attached to the arm, hand, and ball. The markers of the ball were placed

⁹Please note this is a simplified view on the structure, which was chosen for better understanding.

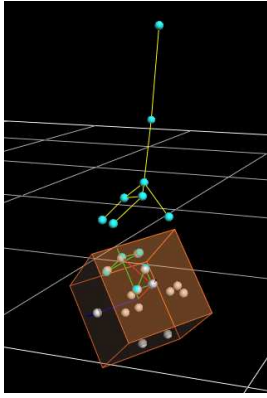


Fig. 9. Sample data of a tracked pose visualized in ViconIQ.

such that both, its position and orientation could be extracted despite coverage during hand contact. Figure 9 depicts a sample of the measured position (upper) and velocity (lower) for the ball and three hand markers. In Figure 10 some sample cycles of the tracked data are shown. Interesting to notice is that besides the vertical motion the hand also performs a rotation around the radial axes of the hand (see also Fig. 11). This is also observed from the velocity plot, where the wrist and knuckle of the middle finger stop accelerating at the end of the hand contact. Then, the fingertip guides the ball and injects the most significant amount of energy into it.

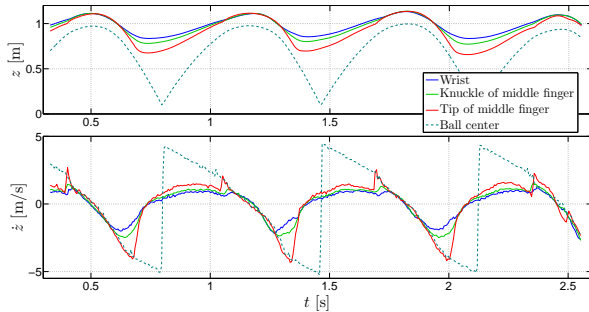


Fig. 10. Position and velocity for a sample dribbling measurement of a semi-pro human player.

The mentioned wrist rotation is also visible in Fig. 11, where the arm motion is shown along the time axis. The indicated points from top to bottom are the shoulder, elbow, wrist, knuckle of middle finger, and tip of the middle finger. It is clear that the two lowest lines, which represent the palm and the finger, are rotating.

The simulation results shown next are planar, i.e. the ball has 3 DoF. The robot is modeled as a velocity source on which the elastic finger is mounted. Basically, we lock the adaptation of the translation in x direction and the rotations about the y and z axis in the model from Sec. II.

B. Simulation with a 3 DoF ball in 2D space

For this first simulation, we assume the robot to be a position/velocity force (i.e. ideal dynamic trajectory track-

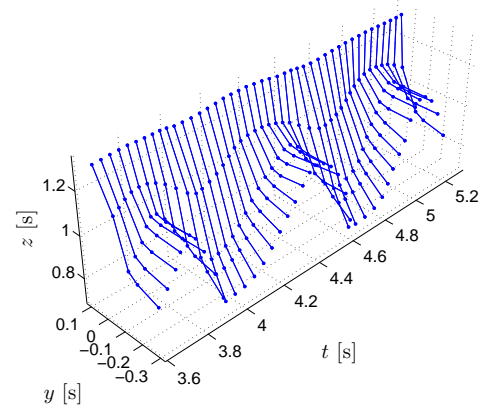


Fig. 11. Tracked arm/hand configuration for human dribbling of a semi-pro human player.

ing)¹⁰. Figure 12 depicts the resulting ball, observer, and hand motion. In the upper plot the lateral position is shown. The steady state point of the ball is located at $d_B = 0$. The hand is expressed in $\{EE\}$, which leads to the shift of the hand with respect to the ball (finger length). Clearly, the ball stabilizes at the desired position. In the lower plot the vertical position is depicted. Also in this direction we obtain a stable cycle for the ball motion. Furthermore, we see that the observer converges within two cycles towards the true ball trajectory.

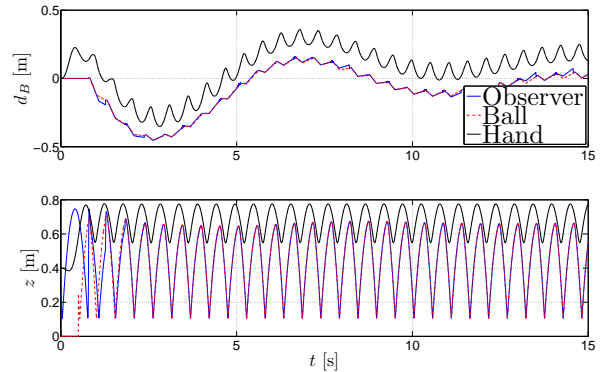


Fig. 12. Position for a simulation with a 3 DoF ball. The upper plot shows the distal coordinate, while the lower one depicts the actual dribbling motion.

C. Simulation with a 6 DoF ball in 3D space

The simulation results presented now are done with the full dynamic model of the LWR-III (see Sec. II-E) that is controlled via Cartesian impedance control (see Sec. III-C).

Figure 13 depicts the ball and hand position in $\{W\}$ again for a regulation dribbling task, however, for a full simulation of robot and impedance controller. Please note that the same y -axis offset as for the 3-DoF simulation is present. As one

¹⁰In all simulations and experiments we use following material parameters for calculating the reflected contact stiffness: $E = 210000 \text{ N/mm}^2$, $I_y = bh^3/12$, $b = 30 \text{ mm}$, and $h = 1 \text{ mm}$.

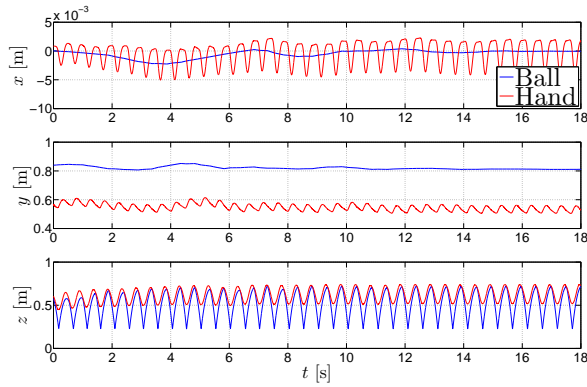


Fig. 13. Relevant ball coordinates for a full dynamic simulation (robot modeled as a flexible joint robot, full-state feedback controller for the motor, and overlaid Cartesian impedance controller) with a 6 DoF ball.

can see the motion converges quickly to the desired stable dribbling cycle in all three axes. Figure 14 shows the contact forces expressed in $\{EE\}$. The maximal contact force is ≈ 20 N along the x -axis. The forces in the z -axis are caused by the friction of the ball.

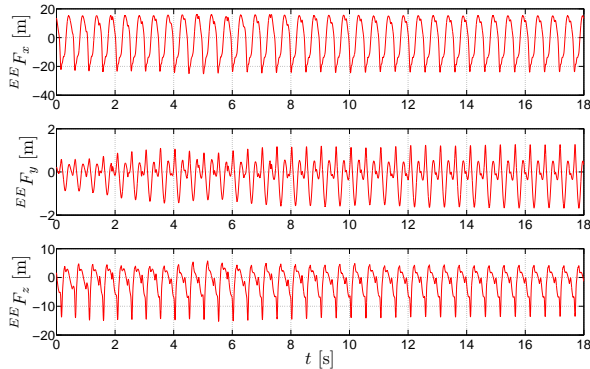


Fig. 14. Contact forces for a full dynamic simulation (robot modeled as a flexible joint robot, full-state feedback controller for the motor, and overlaid Cartesian impedance controller) with a 6 DoF ball.

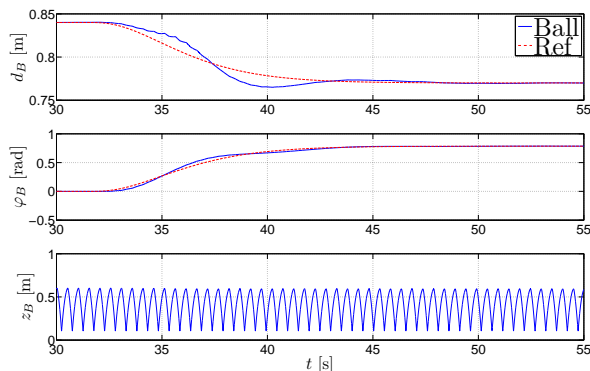


Fig. 15. Relevant ball coordinates for a tracking dribbling simulation (online setpoint adjustment) with a 6 DoF ball.

Figure 15 shows that it is possible also to vary the

lateral set-point and desired distal point online, i.e. with the designed controller the robot is able to follow a desired dribbling trajectory $[d_B(t), \varphi_B(t)]$ without destabilization. The possible online adjustment of dribbling frequency, dribbling height, and amplitude is not shown for brevity. However, this can be viewed in the video. In the depicted simulation the robot performs a simultaneous rotation of 45° and distal motion of 7 cm. Clearly, the dribbling cycle is maintained.

The experimental validation with the LWR-III that is equipped with an elastic hand is described next.

D. Experiments

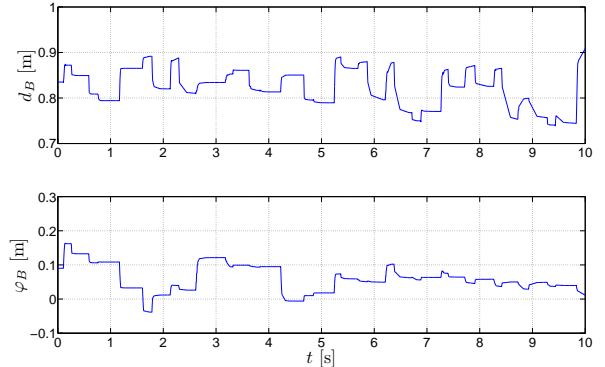


Fig. 17. Distal coordinate d_B and rotation φ_B measured for the LWR-III dribbling experiment.

Figure 16 shows an image series of successful elastic dribbling with a LWR-III. The utilization of the elastic fingers can be clearly observed. A sample measurement is depicted in Fig. 17 and Fig. 18. In the first figure the ball position in cylindrical coordinates d_B and φ_B is shown. In the second figure we find the disturbance compensated end-effector forces. The maximal force in the upper plot is in a similar range as for the 6 DoF simulation, see Fig. 14. Furthermore, the finger oscillations can be observed mainly in x direction of $\{EE\}$. Overall, the robot is able to stabilize the motion of the ball. As one can see in the attached video¹¹ reacts to disturbances (model uncertainties).

V. CONCLUSIONS

In this paper we showed the results of stable dribbling with an intrinsically compliant robot. Based on force sensing and associated ball observation only, we are able to reactively adjust the robot motion such that system errors (ball, robot, and sensing uncertainties) can be coped with. The robustness of the proposed method, which incorporates intrinsic contact compliance and resulting energy transfers, shows the large benefit one can gain from intrinsically compliant actuation in terms of cycle stability, robustness, and manipulability.

A video showing the simulation and experimental results is provided as a video attachment or can be downloaded from <http://www.safe-robots.com/dribbling.html> at higher resolution.

¹¹You can also find a higher resolution version at <http://www.safe-robots.com/dribbling.html>.

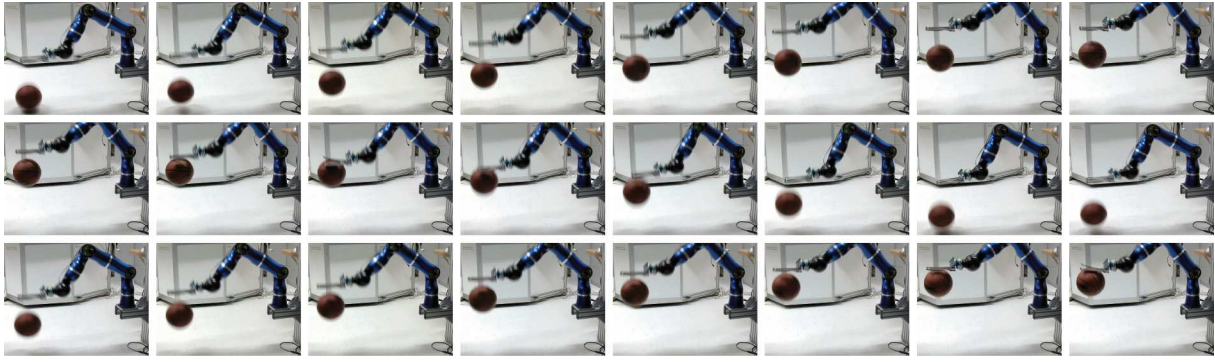


Fig. 16. Snapshots from basketball dribbling with the LWR-III that is equipped with an elastic hand.

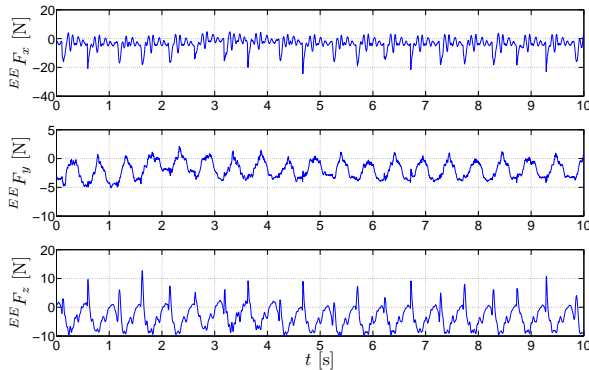


Fig. 18. Experiment force x .

VI. ACKNOWLEDGMENTS

This work has been partially funded by the European Commission's Sixth Framework Programme as part of the project VIATORS under grant no. 231554. We would like to thank Tim Rokahr for his contribution to the mechanical design of the hand.

REFERENCES

- [1] A. Albu-Schäffer, S. Haddadin, C. Ott, A. Stemmer, T. Wimböck, and G. Hirzinger, "The DLR lightweight robot - lightweight design and soft robotics control concepts for robots in human environments," *Industrial Robot Journal*, vol. 34, no. 5, pp. 376–385, 2007.
- [2] S. Haddadin, K. Krieger, and A. Albu-Schäffer, "Exploiting elastic energy storage for cyclic manipulation: Modeling, stability, and observations for dribbling," in *submitted to: IEEE Conference on Decision and Control*, Orlando, USA, 2011.
- [3] M. Stilman. (without date) Mike stilman: Previous projects. Visited on 28th of february 2011. [Online]. Available: <http://www.cc.gatech.edu/~mstilman/earlier.html>
- [4] D. Shiokata, A. Namiki, and M. Ishikawa, "Robot dribbling using a high-speed multifingered hand and a high-speed multifingered hand and a high-speed vision system," in *2005 IEEE International Conference on Intelligent Robots and Systems*, Edmont, Canada, 2005, pp. 3945 – 3950.
- [5] G. Bätz, M. Sobotka, D. Wolherr, and M. Buss, "Robot basketball: Ball dribbling - a modified juggling task," in *2008 IEEE International Conference on Robotics and Automation*, San Diego, USA, 2009, pp. 2410 – 2415.
- [6] U. Mettin, A. S. Shiriaev, G. Bätz, and D. Wolherr, "Ball dribbling with an underactuated continuous-time control phase," in *2010 IEEE International Conference on Robotics and Automation*, Anchorage, USA, 2010, pp. 4669 – 4674.
- [7] M. Bühler, D. E. Koditschek, and P. Kindlmann, "A one degree of freedom juggler in a two degree of freedom environment," in *Proceedings of the International Workshop on Intelligent Robots*, Tokyo, Japan, 1988, pp. 91 – 97.
- [8] R. Ronsse, P. Lefevre, and R. Sepulchre, "Rhythmic feedback control of a blind planar juggler," *IEEE Transactions on Robotics*, vol. 23, no. 4, pp. 790–802, 2007.
- [9] P. Reist and R. D'Andrea, "Bouncing an unconstrained ball in three dimensions with a blind juggling robot," in *2009 IEEE International Conference on Robotics and Automation*, Kobe, Japan, May 2009, pp. 1774 – 1781.
- [10] S. Haddadin, M. Weis, S. Wolf, and A. Albu-Schäffer, "Optimal control for maximizing link velocity of robotic variable stiffness joints," in *accepted at: IFAC World Congress*, 2011.
- [11] J. Yamaguchi, D. Nishino, and A. Takanishi, "Realization of dynamic biped walking varying joint stiffness using antagonistic driven joints," in *IEEE Int. Conf. on Robotics and Automation (ICRA1998)*, Leuven, Belgium, 1998, pp. 2022–2029.
- [12] M. Okada, S. Ban, and Y. Nakamura, "Skill of compliance with controlled charging/discharging of kinetic energy," in *IEEE Int. Conf. on Robotics and Automation (ICRA2002)*, Washington, USA, 2002, pp. 2455–2460.
- [13] M. Grebenstein, A. Albu-Schäffer, T. Bahls, M. Chalon, O. Eiberger, W. Friedl, R. Gruber, S. Haddadin, U. Hagn, R. Haslinger, H. Hoepfner, S. Joerg, M. Nickl, A. Nothhelfer, F. Petit, J. Reill, N. Seitz, T. Wimböck, S. Wolf, T. Wuesthoff, and G. Hirzinger, "The dlr hand arm system," in *accepted at: IEEE International Conference on Robotics and Automation*, 2011.
- [14] K. Waldron and J. Schmiedeler, *Springer Handbook of Robotics*, B. Siciliano and O. Khatib, Eds. Springer, 2005.
- [15] K. H. Hunt and F. R. E. Crossley, "Coefficient of restitution interpreted as damping in vibroimpact," *Journal of Applied Mechanics*, vol. 42, pp. 440–445, 1975.
- [16] C. Canudas-de-Wit and P. Tsiotras, "Dynamic tire friction models for vehicle traction control," in *Proceedings of the IEEE Conference on Decision and Control*, Phoenix, USA, 1999, pp. 3746 – 37251.
- [17] K. Gieck and R. Gieck, *Engineering Formulas*. Germering, Germany: Gieck Publishing, 1997.
- [18] D. Gross, W. Hauger, J. Schröder, W. Wall, and J. Bonet, *Engineering Mechanics 2: Mechanics of Materials*. Heidelberg, Germany: Springer, 2011.
- [19] M. Spong, "Modeling and control of elastic joint robots," *IEEE Journal of Robotics and Automation*, pp. 291–300, 1987.
- [20] S. V. Drakunov, "Sliding-mode observer based on equivalent control method," in *Proceedings of the 31st Conference on Decision and Control*, Tuscon, USA, December 1992, pp. 2368 – 2369.
- [21] D. Gross, W. Hauger, and J. Schröder, *Engineering Mechanics 1: Statics*. Heidelberg, Germany: Springer, 2009.
- [22] S. Haddadin, *Towards Safe Robots: Approaching Asimov's 1st Law*. Aachen, Germany: Rheinisch-Westfälische Technische Hochschule Aachen, 2011, PhD Thesis.
- [23] A. Albu-Schäffer, C. Ott, and G. Hirzinger, "A Unified Passivity-based Control Framework for Position, Torque and Impedance Control of Flexible Joint Robots," *The Int. J. of Robotics Research*, vol. 26, pp. 23–39, 2007.